


Multilayered Titanium Carbide MXene Film for Guided Bone Regeneration

This article was published in the following Dove Press journal:
International Journal of Nanomedicine

Jiebing Zhang

Yu Fu

Anchun Mo 

State Key Laboratory of Oral Diseases,
West China Hospital of Stomatology,
Sichuan University, Chengdu, People's
Republic of China

Purpose: MXenes are two-dimensional (2D) materials that are increasingly being applied in biomedical fields. This is ascribed to their good physiochemical properties, unique structure and high biological compatibility. However, the osteogenic activity and suitability of these materials for bone tissue engineering are not clearly understood. Thus, the aim of this study is to evaluate the biocompatibility, osteoinductivity and guided bone regeneration ability of $Ti_3C_2T_x$ MXene in vitro and in vivo.

Methods: Multilayered $Ti_3C_2T_x$ MXene films were prepared and characterized by XRD and SEM. In vitro experiments were performed to evaluate the effect of MXene films on cell adhesion and morphology with SEM and fluorescence microscopy. The cytotoxicity of MXene films was detected with the Live/Dead double-staining tests. The EdU assay was employed to evaluate cell proliferation on MXene films and ALP activity was tested to determine the effect of the films on osteogenic differentiation in vitro. The mRNA expression of osteogenic differentiation-related markers was measured using qRT-PCR. In vivo animal studies were performed in which the MXene films were implanted subcutaneously in rats to evaluate biocompatibility and host tissue response in vivo. In addition, a rat calvarial defect model was established to examine the bone regeneration performance of the $Ti_3C_2T_x$ MXene films. The specimens were analyzed with micro-CT evaluation and histological tests.

Results: The XRD and SEM analyses revealed that the $Ti_3C_2T_x$ MXene film was successfully synthesized. The cellular experiments showed that MXene films were highly cytocompatible and enhanced osteogenic differentiation in vitro. When implanted into subcutaneous sites and calvarial defect sites in rats, MXene films showed good biocompatibility, osteoinductivity and bone regeneration activity in vivo.

Conclusion: In summary, this study presents new applications of MXenes in bone tissue engineering and in guided bone regeneration therapy.

Keywords: $Ti_3C_2T_x$, bone tissue engineering, GBR, osteoinductivity, biocompatibility

Introduction

Guided bone regeneration (GBR) is the most common and reliable therapy used to treat bone defects around dental implants.¹ The GBR method is based on the creation of a closed space by a barrier membrane to protect the newly formed bone from the fast-growing fibrous connective tissue invading the bone defect area. This maximizes the regeneration ability of the bone tissue.² In clinical practice, the barrier membrane is classified into a resorbable and non-resorbable membrane.³ Polymers and titanium have been employed in the fabrication of non-resorbable membranes whereas collagen is used as the main material for the construction of a resorbable membrane.⁴ An ideal GBR membrane should possess properties that

Correspondence: Anchun Mo
State Key Laboratory of Oral Diseases,
West China Hospital of Stomatology,
Sichuan University, Chengdu 610041,
People's Republic of China
Email moanchun@163.com

are suitable for bone regeneration. First, the membrane should have optimal mechanical strength that matches that of natural bone tissue and gingival tissue to keep the bone regeneration space and prevent damage to the surrounding tissue during surgery.⁵ Second, the membrane should induce osteoconductivity and act as a scaffold to promote stem cells attachment and guide the migration of bone cells.⁶ Third, an ideal GBR membrane should provide sufficient osteoinductivity to induce the differentiation of stem cells into osteoblasts.⁷ However, existing GBR membranes have weak structural integrity and sub-optimal osteoinductivity.⁸

In recent years, several two-dimensional materials have been developed for bone tissue applications, such as graphene and its derivatives.^{9,10} Research has revealed that graphene expedites the osteogenic differentiation of human mesenchymal stem cells,¹¹ and pure graphene hydrogel enhances osteogenic differentiation in vitro and in vivo when used as a barrier membrane for GBR.^{12,13}

MXenes are two-dimensional (2D) transition metal carbides and nitrides discovered by scientists at the Drexel University in 2011.^{14,15} $Ti_3C_2T_x$ was the first MXene to be synthesized by etching Al layer in Ti_3AlC_2 , where T_x represents the surface groups (such as -F and -OH) formed during the etching procedure.¹⁶ The new 2D material was named MXene because of its similarities with graphene.¹⁴ MXenes have shown promising performance in many fields, such as environmental science,¹⁷ energy storage,¹⁸ composite materials¹⁹ and many others. MXenes display several features such as high hydrophilicity,²⁰ biocompatibility,^{21,22} biodegradability²³ and antibacterial activity.²⁴ Given these characteristics, there has been great interest to expand the application scope of MXenes to various biomedical research fields,²⁵ including biosensing,^{26,27} antibacterial materials,^{24,28} bioimaging probes^{29,30} and cancer treatment.³¹ Chen et al prepared a OTES- $Ti_3C_2T_x$ /PLA composite membrane and found that the addition of 1 wt.% $Ti_3C_2T_x$ nanosheets enhances cell proliferation and osteogenic differentiation ability of PLA.³² Owing to the good physiochemical performance, unique structure and biological compatibility of 2D materials, we hypothesize that MXenes are suitable for bone tissue engineering application and GBR treatment similar to graphene.

In this work, we use flexible freestanding $Ti_3C_2T_x$ MXene films to evaluate the cytocompatibility and osteoinductivity of $Ti_3C_2T_x$ MXene in vitro. In addition, we investigate the host tissue response and guided bone

regeneration ability of this material in vivo. This is the first study to apply MXenes in bone tissue engineering and GBR therapy.

Materials and Methods

Materials

Ti_3AlC_2 MAX was purchased from 11 Technology Co., Ltd (China). Lithium fluoride (LiF, 98.5%) was purchased from Aladdin Biochemical Technology Co., Ltd (China) and hydrochloric acid (HCl, 37.2%) was from Baoxin Technology Co., Ltd (China). The titanium membranes were of pure commercial quality with a thickness of about 20 μm (Guantai Co., Ltd, China). High-glucose DMEM (Dulbecco's modified eagle medium), penicillin/streptomycin, fetal bovine serum (FBS) were obtained from GIBCO (USA). Triton X-100, β -Glycerophosphate, dexamethasone and L-ascorbic acid were purchased from Sigma-Aldrich Co. (USA). All chemicals were analytically pure and used without further purification.

Preparation of $Ti_3C_2T_x$ MXene Films

MILD method was used to produce $Ti_3C_2T_x$ MXene as previously reported.³³ 0.5 g of Ti_3AlC_2 MAX (400 mesh) was slowly added to the etchant solution prepared by dissolving 0.8 g LiF in 10 mL of 9M HCl in a 50 mL-TEFLON Erlenmeyer flask. The reaction mixture was continuously stirred with a magnetic stirrer and allowed to run in water bath at 35°C for 24 hrs. The acidic product was washed with deionized water (DI H₂O) and then centrifuged (5 mins per cycle at 3500 rpm) several times until pH \geq 6. After decanting the supernatant solution, a sediment with a distinctive black layer was formed above a grayish layer. The black layer slurry ($Ti_3C_2T_x$) was carefully separated with a spatula from the sediment and collected. This was followed by the addition of DI water to the $Ti_3C_2T_x$ slurry and hand-shaking for 5 mins. The suspension was centrifuged (at 3500 rpm for 1 hr) to obtain a colloidal solution of delaminated $Ti_3C_2T_x$ MXene flakes (~ 1 mg/mL). $Ti_3C_2T_x$ MXene films were fabricated via vacuum-assisted filtration through a PVDF filter membrane (0.45 μm pore size). After drying at 120°C for 24 hrs in a vacuum oven, a flexible free-standing multilayered $Ti_3C_2T_x$ MXene film was formed.

Characterization

The surface and cross-section morphology of the MXene films were characterized by scanning electron microscopy

(SEM, Inspect F50, FEI, Hillsboro, US), operated at 20 kV. The chemical composition of $Ti_3C_2T_x$ MAX and $Ti_3C_2T_x$ MXene were analyzed by X-ray diffraction (XRD, Bruker D8 ADVANCE A25X; BRUKER AXS GMBH, Germany) with Cu-K α radiation of 40 kV, 44 mA at room temperature. The XRD patterns were collected in the 2 θ range of 5°–85°. The water contact-angle was tested by an automatic contact angle meter (Model SL200A/B/D Series, Solon Tech. Inc. Ltd., China).

Cell Culture

Mouse preosteoblast cell line MC3T3E1 Subclone 14, purchased from the American Type Culture Collection (CRL-2594; ATCC, USA), was grown in high-glucose DMEM containing 1% penicillin/streptomycin and 10% fetal bovine serum in a humidified incubator with 5% CO₂ at 37°C. The medium was replaced at a 2-days interval. For cell seeding, the MXene films were cut into circular sections of 12 mm diameter attached to 12 mm diameter coverslips by a dental bond (SE BOND, CLEARFIL). The samples were placed in a 24-well plate and sterilized overnight by exposure to UV light and washed three times with PBS.

Cell Adhesion

The MC3T3E1 cells were cultured on MXene films for 24 hrs, then fixed in 2.5% glutaraldehyde overnight at 4°C followed by dehydration with ascending concentration of ethanol (30%, 50%, 75%, 85%, 95% and 100% for 15 mins each). Finally, the samples were sputter-coating with gold and examination with SEM (Inspect F50, FEI, Hillsboro, US) to observe the cell adhesion ability on the MXene films.

Cell Morphology

The morphology of MC3T3E1 cells cultured on MXene films was visualized by labeling the actin cytoskeletons of the cells with Alexa Fluor 488-Phalloidin (Invitrogen, USA). Briefly, the cells were cultured (2×10^4 cells/well) on MXene films and coverslips for 24 hrs. After fixing in 3.7% formaldehyde solution in PBS at room temperature for 15 mins, cells were permeabilized with 0.1% Triton X-100 for 15 mins, blocked with 1% albumin from bovine serum (BSA, Sigma, USA) and stained with Phalloidin-Alexa Fluor 488 for 30 mins to label the F-actin. Lastly, 2-(4-amidinophenyl)-6-indolecarbamidine dihydrochloride (DAPI, sigma, USA) was added to stain cell nuclei. The staining of cytoskeletons of cells was

examined under a fluorescent microscope equipped with a digital camera (Olympus America, USA).

Live/Dead Double Staining

The MC3T3E1 cells were seeded (3×10^4 cells/well) on MXene films and coverslips and incubated for 24 hrs. The cytotoxicity of cells on MXene films was detected by Live/Dead double-staining kit (KeyGen, China). Cells were stained with 2 μ M Calcein-AM and 8 μ M propidium iodide (PI) for 15 mins. Live cells appeared green after Calcein-AM staining, while dead cells appeared red due to PI staining. The stained specimens were observed and imaged under a fluorescent microscope.

Cell Proliferation

The proliferation of cells was determined with an EdU-488 Cell Proliferation Kit (Beyotime, China). This analog of thymidine EdU (5-ethynyl-2'-deoxyuridine) can be incorporated into newly synthesized DNA during active DNA synthesis.³⁴ Briefly, after incubation for 24 hrs, cells were cultured with EdU for 2 hrs and then fixed with 4% paraformaldehyde for 15 mins. The cells were permeabilized with 0.1% Triton X-100 for 15 mins and labeled with Azide 488 for the click reaction for 30 mins. Lastly, Hoechst 33342 reagent was added to stain cell nuclei. Specimens were photographed by a fluorescence microscope. The number of EdU-positive cells (green) and total cells (blue) were counted in five randomly chosen fields. EdU-positive ratio was calculated as the ratio of the number of EdU-positive cells divided by the total number of cells.

ALP Activity Assay

The MC3T3E1 cells were incubated (2×10^4 cells/well) on MXene films and coverslips with either osteogenic medium or growth medium. The osteogenic medium contained 100 nM dexamethasone, 10 mM β -glycerophosphate and 50 μ g/mL L-ascorbic acid. At 4 and 7 days after seeding, Alkaline phosphatase (ALP) activity was measured with commercial ALP assay kit. This assay works on the principle that the conversion of p-nitrophenol phosphate (pNPP) to p-nitrophenol produces a yellowish color when incubated with ALP. At each time point, cells were harvested and lysed with cell lysis buffer. The cell lysate was co-incubated with pNPP at 37°C for 15 mins. The reaction was terminated with the addition of 100 μ L of stop solution. A microplate reader (BioTek ELx808, USA) was used to record the absorbance at 405 nm. Total protein

concentration was determined by BCA assay kit (Beyotime, China), and optical density was read at 562 nm. The results were normalized to the number of millimoles of p-nitrophenol per min per mg of total protein (mmol/min/mg protein). All experiments were performed in triplicate.

qRT-PCR

The relative mRNA level of marker genes was measured by real-time reverse transcriptase polymerase chain reaction (qRT-PCR). Cells were cultured on MXene films and coverslips at density of 2×10^4 cells/well in osteogenic medium. At 4 and 7 days of culture, total RNA was isolated using Trizol reagent (Invitrogen, USA). The RNA was used to synthesize complementary DNA (cDNA) with an RT6 cDNA Synthesis Kit (TsingKe, China). qRT-PCR reactions were performed with a T5 Fast qPCR Mix SYBR Green I (TsingKe, China) and ABI 7300 (Applied Biosystems, China). After 1 min of preincubation at 95°C, 40 amplification cycles were performed. Each cycle consisted of the following two steps: 10 s at 95°C and 15 s at 60°C. The primer sequences of the genes are as follows: β -actin: F-5'-AGATTACTGCTCTGGCTCCTAGC-3', R-5'-ACTCATC GTACTCCTGCTTGCT-3'; ALP: F-5'-CTGCCTGAAAC AGAAAGTCTGC-3', R-5'-TATGTCTTTACCAGGAGGC GTG-3'; OCN: F-5'-GGACCATCTTTCTGCTCACTCTG -3', R-5'-ACCTTATTGCCCTCCTGCTTG-3'; and OPN: F-5'-TTCTCCTGGCTGAATTCTGAGG-3', R-5'-GCTGC CAGAATCAGTCACTTTC-3'.

Subcutaneous Implantation Procedures

MXene films were cut into 7 mm diameter circles and implanted in mice to investigate the host tissue response. Three male Sprague-Dawley rats (SD rats) aged 8 weeks were used for this purpose. This experimental protocol was approved by the Research Ethics Committee of West China School of Stomatology and strictly followed the national standards "Laboratory Animal Requirements of Environment and Housing Facilities (GB 14925-2001)". MXene films were implanted into 3 subcutaneous dorsum sites of each rat. Rats were sacrificed at 2 weeks after surgery and MXene films with the surrounding tissue were harvested and fixed in 4% paraformaldehyde solution. The specimens were embedded in paraffin, vertically sectioned into 5 μ m-thick slices and stained with hematoxylin and eosin (HE) for histological evaluation. Images were taken using an Olympus light microscope.

Rat Calvarial Defect Model Procedures

Thirty-six male SD rats aged 8 weeks were used to establish a rat calvarial defect model.³⁵ All SD rats were randomly divided into 3 groups: control group with empty bone defects (n = 12); MXene film group (n = 12); titanium membrane group (n = 12). Briefly, after anesthetization and exposure of cranium, two critical-sized bone defects were made on the bilateral sides of the cranial sagittal suture in each rat using a dental trephine drill (5 mm diameter) cooled with saline.¹³ The bone defects were completely covered with test GBR membranes of about 7 mm diameter. In the control group, the defects were left empty. Then, the wounds were sutured carefully. At 4 weeks and 8 weeks after surgery, the rats were sacrificed and the skulls were harvested and fixed in 4% paraformaldehyde solution for analysis.

Micro-CT Evaluation

The micro-CT images were captured using a micro-CT scanner (μ CT 80; Scanco Medical, Switzerland) set to a voltage of 70 kV and a current of 200 μ A. MIMICS (Materialise, US) was used to obtain 3D reconstruction images from micro-CT scans. BoneJ was employed to determine the micro-morphometric bone parameters including the bone volume fraction (BVF) calculated as the bone volume (BV, mm^3) per tissue volume (TV, mm^3), trabecular thickness (Tb.Th, mm) and trabecular separation (Tb.Sp, mm).³⁶ The region of interest (ROI) was a cylindrical region (5 mm diameter) covering the entire thickness of the calvarial bone height.

Histological Analysis

After Micro-CT scanning, the specimens were dehydrated and embedded in methylmethacrylate. They were sectioned into 50 μ m-thick slices in coronal plane from the center of the defects with a rotary cutting observer (SP1600, Leica Microsystems, Germany). Subsequently, the sections were stained with Van Gieson's picric acid-fuchsin staining solution.³⁷ The sections were observed using an Olympus light microscope.

Statistical Analyses

All measurements are presented as mean \pm standard deviation. The data were analyzed with Prism software (GraphPad, IL). Student's *t*-test was used to compare independent samples between two groups and the one-way analysis of variance (ANOVA) were employed to compare

multiple groups. The statistical significance was considered at $*p<0.05$, $**p<0.01$, $***p<0.001$ and $****p<0.0001$.

Results and Discussion

Preparation and Characterization of MXene Film

The $Ti_3C_2T_x$ MXene was synthesized using the MILD method as described previously.³³ After etching and drying, the flexible freestanding multilayered $Ti_3C_2T_x$ MXene film could be easily peeled off from the filter membrane (Figure 1A). The MXene film weighed about 50 mg, with a thickness of about 40 μm . The multilayered MXene structure was characterized using X-ray diffraction (XRD) and scanning electron microscopy (SEM). The cross-section SEM image of dried sample displayed a unique multilayered stacked structure (Figure 1B), and the surface morphology was rough and disorderly (Figure 1C). Materials with rough surfaces are suitable for cell attachment, proliferation and bone cell differentiation.³⁸ Moreover, the dense multilayered stacked structure of $Ti_3C_2T_x$ made it an effective barrier for a GBR membrane to stop fibroblast migration. The XRD

pattern of $Ti_3C_2T_x$ (Figure 1D) revealed the disappearance of Ti_3AlC_2 peaks and only intensive (002) peak. The XRD pattern matched with previous reports,¹⁶ indicating that the $Ti_3C_2T_x$ MXene was successfully etched and synthesized. The water contact angle on MXene films was $39.47 \pm 3.12^\circ$ (Figure 1E) as revealed by drop-shape analysis. The lower water contact angles indicate that the surface of MXene films is hydrophilic due to functional groups on $Ti_3C_2T_x$ surface. This hydrophilicity promotes cell attachment and cell spreading as reported in many studies.³⁹ These properties indicate the application potential of MXene in GBR therapy.

Cell Adhesion, Morphology, Cytotoxicity and Proliferation on MXene Film

The cytocompatibility of MXene films was evaluated using the mouse preosteoblast cell line MC3T3E1 Subclone 14. The effect of MXene films on cell adhesion and cell morphology was analyzed by SEM. As shown in Figure 2A, cells appeared round on coverslips but were flatter with wider cytoplasmic extensions and numerous

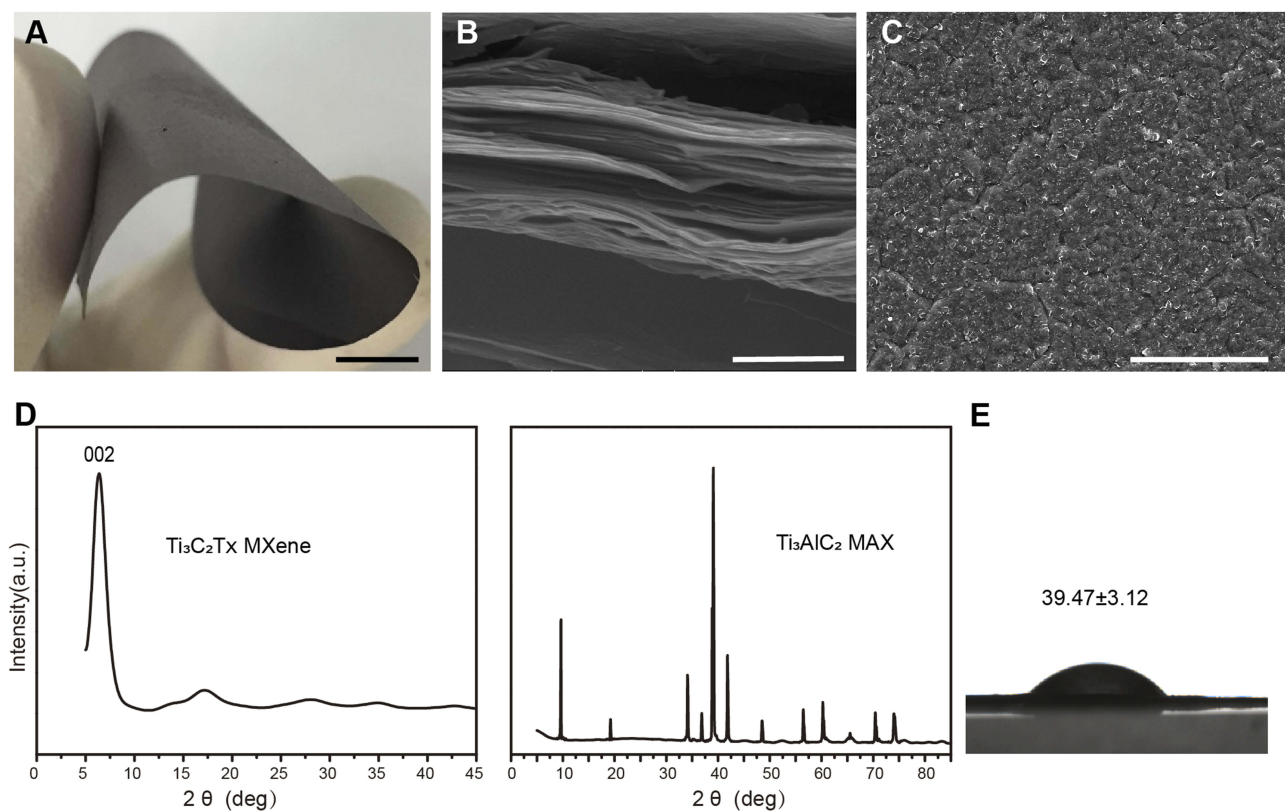


Figure 1 Characterization of multilayered $Ti_3C_2T_x$ MXene films. (A) Photograph of the flexible freestanding MXene film. Scale bars: 5 mm (B) SEM image of the cross-section of MXene films. Scale bars: 1 μm . (C) SEM image of MXene films surface. Scale bars: 50 μm . (D) XRD pattern of $Ti_3C_2T_x$ MXene and Ti_3AlC_2 MAX. (E) Water contact angles on $Ti_3C_2T_x$ MXene films ($n=3$).

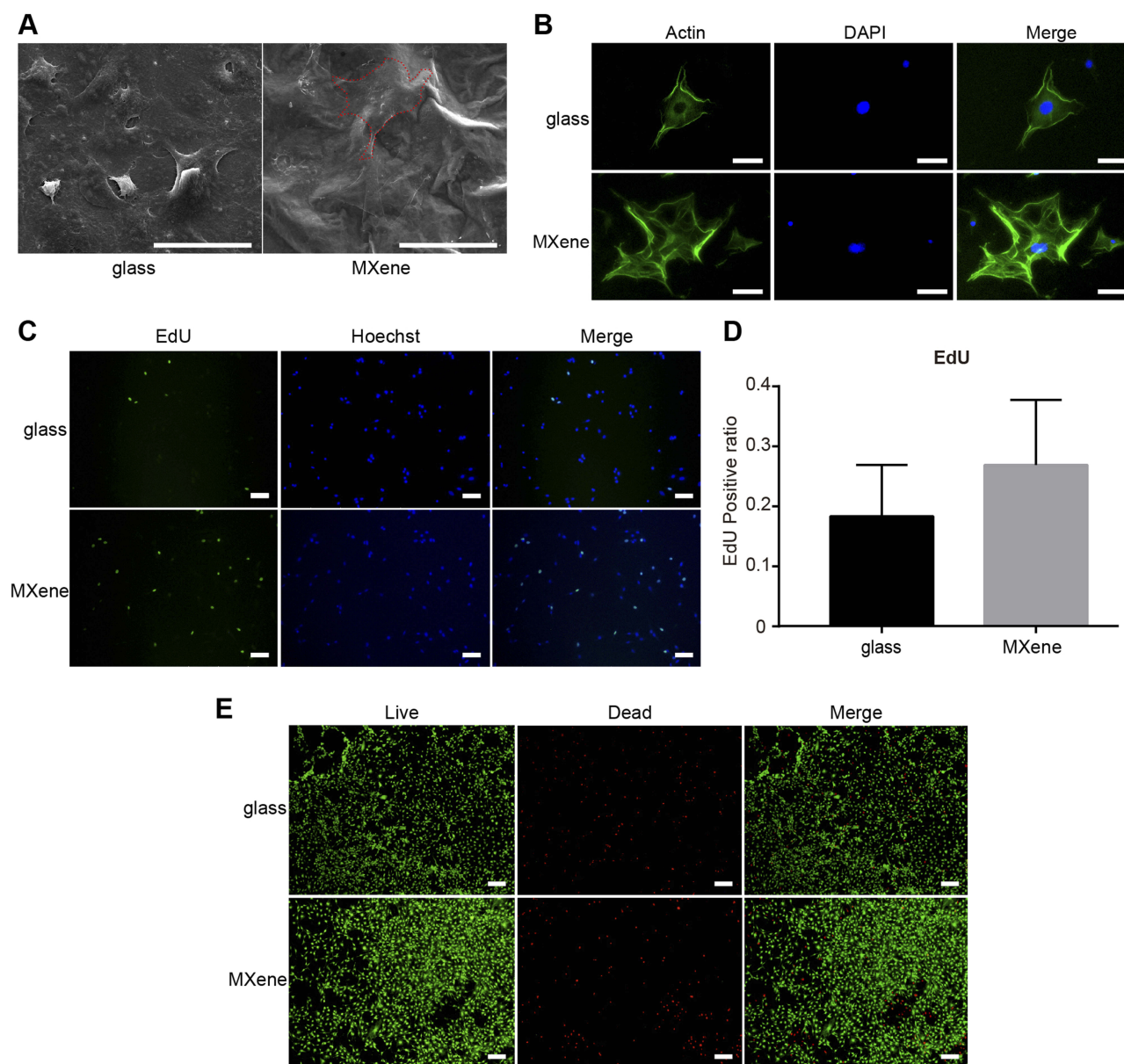


Figure 2 Cell adhesion, morphology, cytotoxicity and proliferation on MXene films. **(A)** Representative SEM images of cells attached on coverslips and MXene films surface after culturing for 24 hrs. Scale bars: 50 μm . **(B)** Representative images of cell morphology of cells seeded on MXene films and coverslips for 24 hrs. Green staining shows the cytoskeleton and blue staining indicates the nuclei. Scale bars: 50 μm . **(C)** Images of cells cultured on coverslips and MXene films for 24 hrs. The proliferating cells are labeled with EdU (green), nuclei are stained blue with Hoechst 33342. Scale bars: 100 μm . **(D)** EdU-positive ratio, calculated by counting the number of EdU-positive cells (green) per the total number of cells (blue), for cells cultured on coverslips and MXene films for 24 hrs. (n=5) **(E)** Live/Dead double staining, cells on coverslips and MXene films 24 hrs after seeding. Red staining represents dead cells while green fluorescence indicates live cells. Scale bars: 200 μm .

filopodia attachment after culturing on MXene films for 24 hrs. The SEM images indicated that $\text{Ti}_3\text{C}_2\text{T}_x$ enhanced the adhesion and adaptation of the cells. After incubating the cells on MXene films and coverslips for 24 hrs, the cell morphology was also observed by a fluorescence microscope. The filamentous actin of the cytoskeleton was stained green with Alexa Fluor 488-Phalloidin and nuclei were stained blue with DAPI (Figure 2B). Relative to the morphology of cells on coverslips, cells incubated on

MXene films appeared flatter, with wider spreading and many filopodia. Previous reports indicate that wider cell spreading and formation of many filopodia promotes osteogenic differentiation of stem cells.⁴⁰ The cells were subjected to the Live/Dead double-staining for 24 hrs to determine the cytotoxicity of MXene films. Results showed that live cells appeared green due to Calcein-AM staining and the dead cells appeared red because of propidium iodide staining. The majority of cells attached on the

MXene films were alive (green), and only a few cells died (red). The fluorescence microscopic images (Figure 2E) revealed that the density of live cells was not markedly different between cells incubated on the glass and those incubated on MXene films. These results show that the $Ti_3C_2T_x$ MXene films are not cytotoxic. Furthermore, we performed the EdU assay to evaluate cell proliferation on MXene films. In this assay, the analog of thymidine EdU (5-ethynyl-2'-deoxyuridine) was incorporated into the newly synthesized DNA. After incubating cells on MXene films and coverslips for 24 hrs, we stained the proliferating cells green with EdU by the click reaction, while the nuclei were stained blue with Hoechst 33342. The fluorescence microscopic images (Figure 2C–D) showed that there was no significant difference in the EdU-positive ratio between the substrates, and it was slightly higher on MXene films. This result indicates that MXene films do not inhibit the proliferation of cells. The CCK-8 assay is commonly used to assess cell proliferation. However, in this study, this method yielded high

absorbance values. This may be due to the functional groups on $Ti_3C_2T_x$ surface which reduce WST-8 and confer them with a yellow-color formazan dye. This result indicates that $Ti_3C_2T_x$ is reducible and thus not suitable for this type of cell proliferation assay. Various aspects of materials that affect the cells include surface topography, chemistry or surface energy. These in vitro tests demonstrate that the $Ti_3C_2T_x$ MXene films are highly cytocompatible and are suitable for cell proliferation, which may be attributed to its rough morphology and hydrophilic surface functional groups.

Osteogenic Differentiation of MC3T3E1 on MXene Film

The effect of MXene films on osteogenic differentiation in vitro was detected using the MC3T3E1 cell line, because of its high osteogenic differentiation potential.⁴¹ Alkaline phosphatase (ALP) is a common marker of early osteoblastic differentiation of bone cells. Figure 3A shows the ALP activity of cells cultured on coverslips and MXene films for

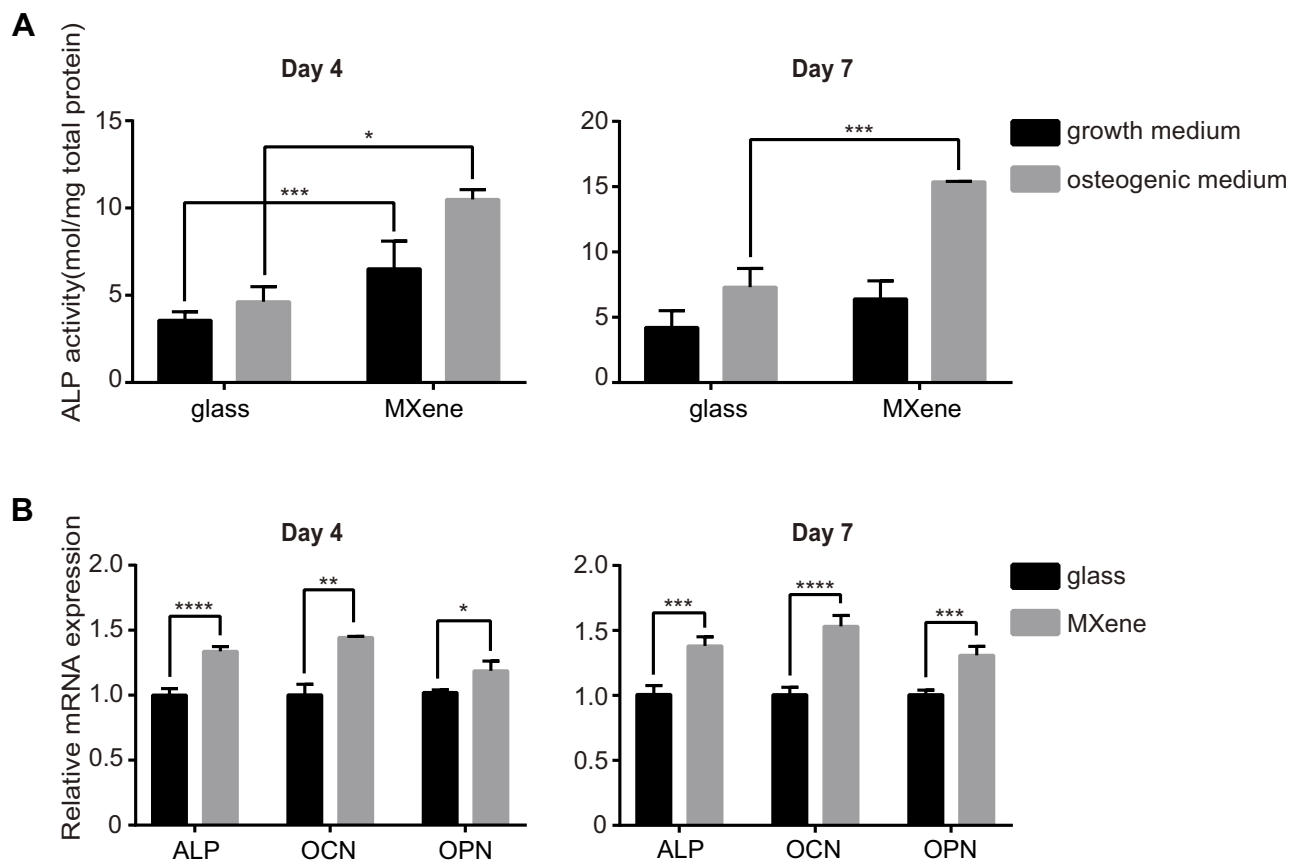


Figure 3 Enhanced osteogenic differentiation of MC3T3E1 cells cultured on MXene films. (A) The ALP activity of cells grown on coverslips and MXene films at 4 and 7 days after seeding in osteogenic medium or growth medium. (B) mRNA levels of the osteogenic differentiation-related genes ALP, OCN and OPN in cells cultured on coverslips and MXene films at 4 and 7 days after seeding in osteogenic medium. (* $p < 0.05$, ** $p < 0.01$, *** $p < 0.001$ and **** $p < 0.0001$).

4 and 7 days. Compared to the cells grown on glass, the ALP activity of MXene group was noticeably higher on day 4, both in osteogenic medium or growth medium. The ALP activity of cells grown on MXene films with osteogenic medium for 7 days was higher relative to that of cells grown on glass with osteogenic medium. The osteogenic differentiation of cells cultured on MXene films was also evaluated by qRT-PCR. The mRNA level of the osteogenic differentiation-related genes ALP, osteocalcin (OCN) and osteopontin (OPN) were measured at day 4 and day 7 in cells seeded on coverslips and MXene films in osteogenic medium (Figure 3B). After culturing for 4 days and 7 days, it was found that the mRNA level of ALP, OCN and OPN were remarkably higher in cells grown on MXene films than those grown on glass groups. In addition, the results of ALP activity test and qRT-PCR indicated that $Ti_3C_2T_x$ MXene enhanced the osteogenic differentiation of preosteoblasts even in the absence of osteogenic medium. Notably, difference between the substrates was significant at early stages (at day 4), but diminished in growth medium over time. At 7 days, the ALP activity of cells grown on MXene films in the growth medium was similar to that of cells cultured on coverslips. This result may be due to the downregulation of cell proliferation of MC3T3E1 and the mechanism of osteoinductivity of MXene films. After 7 days of culture in the growth medium, the MC3T3E1 cells reached confluence and underwent growth inhibition. As previously reported,⁴² downregulation of cell proliferation of MC3T3E1 may cause spontaneous osteogenic differentiation and upregulation of ALP production. The production of ALP may diminish the difference between the MXene group and the control group. Second, the osteogenic differentiation of MC3T3E1 on MXene films may be influenced by the surface morphology and functional groups of the films. It should be noted that the functional groups of $Ti_3C_2T_x$ introduce negative charges to MXene films surface,⁴³ creating an electrically charged microenvironment, which is suitable for bone defect healing as demonstrated in previous reports.⁴⁴ Moreover, the hydroxy groups on $Ti_3C_2T_x$ may form hydrogen bonds with proteins and thus influence cell differentiation. Previous studies reported that multilayered $Ti_3C_2T_x$ MXene undergoes gradual oxidation and degradation in water.⁴⁵ Along the incubation period, oxidation and degradation processes may alter the surface morphology and functional groups on $Ti_3C_2T_x$. This may explain the decrease in the ability of MXene films to stimulate osteogenic differentiation over time.

Host Tissue Response to MXene Film in vivo

To evaluate the biocompatibility and host tissue response to the MXene film in vivo, we implanted the MXene films subcutaneously in rats. Two weeks after surgery, all rats recovered well. Cracked MXene films were observed in subcutaneous tissue by histological examination. As shown in Figure 4A–B, HE staining showed a mild inflammatory response, as evidenced by the formation of granulation tissue around the cracked MXene films accompanied by many fibroblasts and capillary vessels. No noticeable inflammatory cell infiltration and necrosis were observed. Macrophages were attached to the MXene films, indicating the initial stage of biodegradation. The MXene films were actively absorbed by cell-mediated phagocytosis. These results reveal that $Ti_3C_2T_x$ are highly biocompatible with a good biodegradation profile for in vivo application.

Bone Regeneration Performance of MXene Film in vivo

We further explored the ability of $Ti_3C_2T_x$ MXene to promote bone regeneration using a rat calvarial defect model (Figure 5A). It is known that the 5 mm critical-sized defect

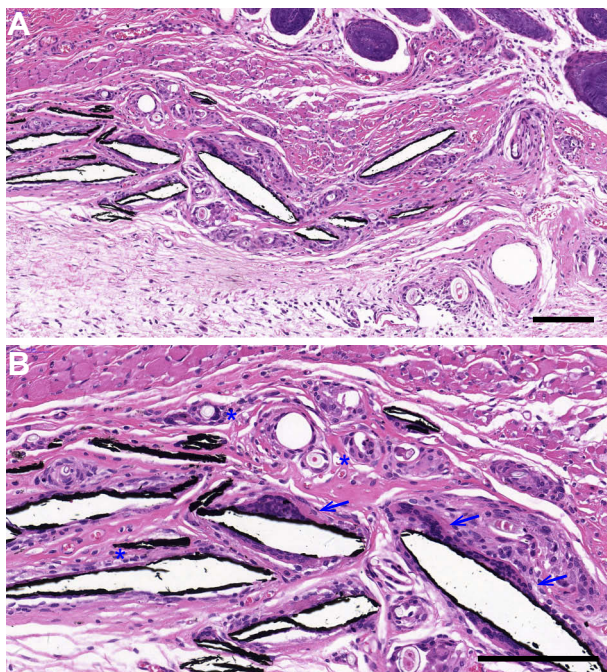


Figure 4 The host tissue response to MXene films. Histological sections of the tissue surrounding the MXene films after HE staining, 2 weeks after surgery. Macrophages (blue arrows) and many blood vessels (blue asterisks) were observed around the cracked MXene film chips. Blue arrows mark the macrophages and blue asterisks mark the blood vessels. Low magnification (A) Scale bar: 150 μ m and high magnification (B) Scale bar: 50 μ m.

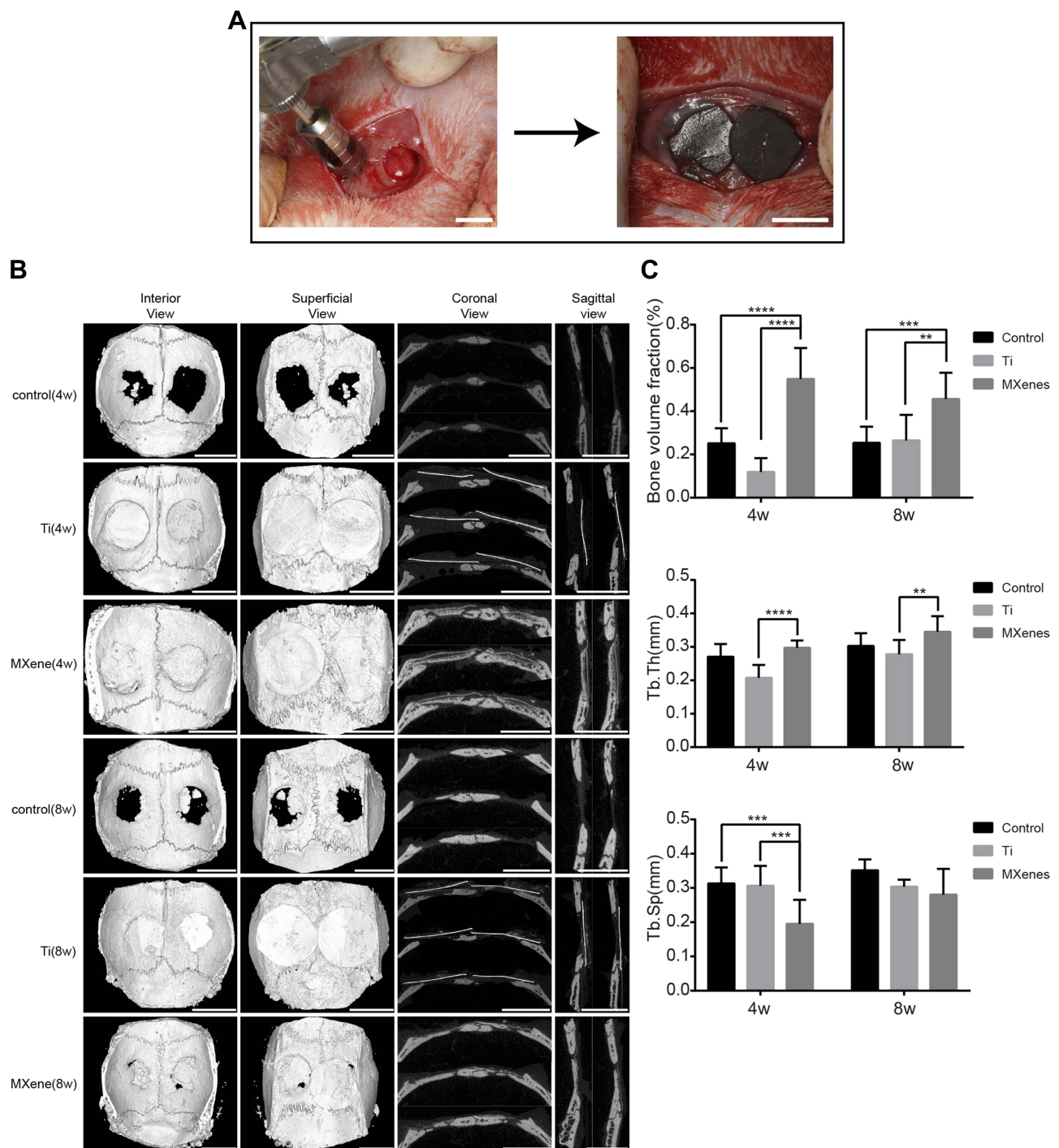


Figure 5 The bone regeneration performance of MXene film *in vivo*. **(A)** Surgical operation to create rat calvarial defect model and to cover the bone defects with MXene films. Scale bars: 5 mm. **(B)** Micro-CT reconstruction images of bone defect samples including interior, superficial, coronal and sagittal views at the 4th and 8th week after surgery. Scale bars: 5 mm. **(C)** Bone morphometric parameters including BVF, Tb.Th and Tb.Sp at 4 and 8 weeks after surgery. Note that BVF was significantly higher in MXene film group than in other groups. (** $p < 0.01$, *** $p < 0.001$ and **** $p < 0.0001$).

Abbreviations: NB, new bone; Ti, titanium; Tb.Sp, trabecular separation; Tb.Th, trabecular thickness.

on the rat cranium does not recover throughout the rats' lifetime due to poor blood supply.³⁵ Titanium membranes, which are used as GBR membranes in clinical practice, served as the positive control group. In surgery, the

hydrophilic surface of the MXene films made them adhere well to the bone tissue around the defect. All rats were in good health condition throughout the 8-weeks healing period and there was no evident infection or complication. At 4 and

8 weeks after surgery, gross observation showed that the titanium membrane was not at the same implantation site or was not adherent to the tissues, indicating loss of flexibility and mechanical compatibility with the surrounding tissues. Analysis of the MXene films revealed the presence of cracks and structural alterations. This result suggested that the bonding between the layers of $Ti_3C_2T_x$ MXene sheets weakened, degraded and dispersed into the body fluids over time.

Micro-CT Evaluation

To assess the amount and quality of the newly formed bone, the micro-computed tomography (Micro-CT) scanning was carried out at 4 and 8 weeks after surgery. The reconstruction images (Figure 5B) of calvarial specimens showed that new bones were formed in the defect site under MXene films. The uniform and continuous new bone almost completely healed the bone defects. In addition, the images showed that the new bone extended from the defect margins and formed bone islands under MXene films. These results indicated that MXene films guided the bone tissue extension from the defect margins and induced new bone formation. Compared to MXene films, only a slight bone regeneration was observed near the defect margins in the control group and titanium membrane group, and there was no continuous healing in the central region of the defect. The micro-morphometric bone parameters (Figure 5C) obtained with BoneJ were in agreement with the micro-CT images.³⁶ At 4 and 8 weeks, MXene film group exhibited remarkably larger bone volume fraction (BVf, BV/TV) in comparison to the control group and titanium membrane group. The BVf of MXene films was not significantly different between 4 weeks and 8 weeks, showing that the majority of bone tissue regeneration occurred in the early stages. According to the BVf results, the MXene films increased the amount of bone regeneration, an effect ascribed to the presence of $Ti_3C_2T_x$ MXene. The quality of newly formed bone was assessed by the trabecular separation (Tb.Sp) and the trabecular thickness (Tb.Th). Tb.Th was not significantly different between MXene films and the control group. As previously reported, the trabecular thickness is commonly used to describe cancellous bone.⁴⁶ However, new bones formed on rat skull are mainly composed of dense cortical bone. Therefore, the Tb.Th is not suitable for evaluating the quality of new bone in rat calvarial defect model. Notably, among the three groups, the MXene film group had the smallest Tb.Sp value at 4 weeks, but the value was not significantly different among the 3 groups at 8 weeks. This indicated that the initial new bone formed

under MXene films was more mature and denser relative to the control and titanium membrane groups. The titanium membrane group had smaller BVf and Tb.Th than other groups. This may be caused by the potential detachment of titanium membranes from the bone defect and the inhibition of new bone growth by the fast-growing fibrous connective tissue into the bone-defected area. The poor performance of the titanium membrane indicated that the mechanical property of the GBR membranes should be compatible with the osseous and surrounding tissues.

Histological Analysis

Undecalcified histological sections were used to perform a histological assessment of the rat calvarial defect model based on Van Gieson's staining (Figure 6). At 4 weeks and 8 weeks after surgery, the histological analysis showed that nearly all the defect space under MXene films was filled with new bone without inflammatory reactions. The regenerated bone had a flattened and uniform structure. MXene films did not integrate with the osteoid tissue, instead a thin collagen fiber separated them. The volume of the new bone in MXene group was remarkably larger than that of the control group. Moreover, the bone defects were only covered with a thin connective tissue and there was no bone regeneration in the central region of the defect site in the control group. The bone lamella structure at 8-weeks was more mature and similar to the normal bone under MXene films compared with at 4-weeks. In addition, the newly formed medullary cavity was smaller at 8 weeks than at 4 weeks. These results show that the MXene films have a high bone regeneration ability in vivo, by providing sufficient osteogenesis space, faster mineralization and early osteogenesis. But MXene films have some limitations when used as a barrier membrane in GBR. The mechanical strength of MXene films decreases in the body fluid environment, and this may be as a result of being redispersed and degraded in the body. We plan to develop a composite based on $Ti_3C_2T_x$ MXene to improve its mechanical properties for GBR application.

Conclusion

In summary, the application potential of multilayered $Ti_3C_2T_x$ MXene films in GBR is investigated in this study. Cellular experiments show that $Ti_3C_2T_x$ MXene has good cytocompatibility, cell spreading and proliferation. The results of ALP assay and qRT-PCR show that MXene enhances osteogenic differentiation of preosteoblast cells in the early stages. The host tissue response to MXene films confirms that the $Ti_3C_2T_x$ MXene films have no

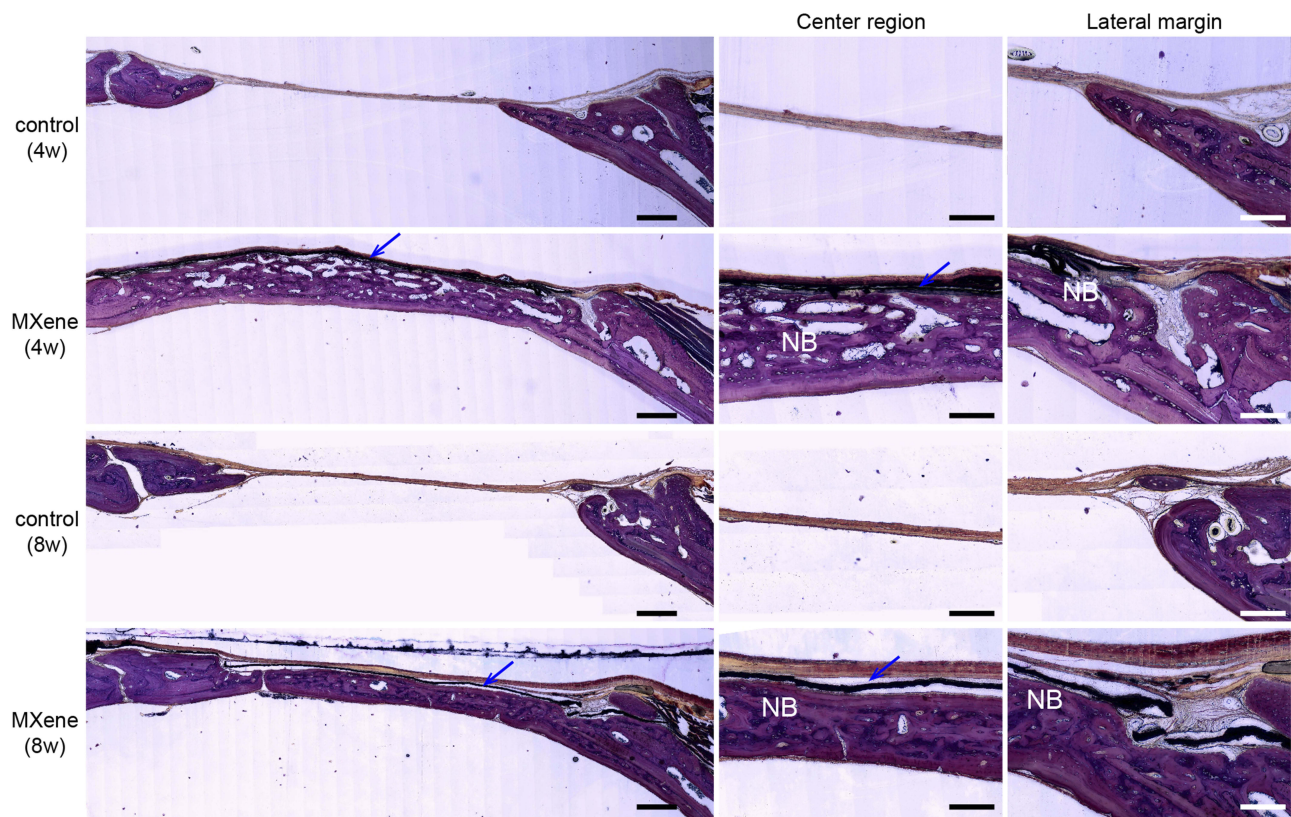


Figure 6 Undecalcified histological sections of calvarial samples 4 and 8 weeks after surgery following Van Gieson's staining. Left images show the volume of newly formed bone with/without MXene films at low magnification. Scale bars: 500 μ m. Right images show the newly formed bone (NB) in the central region and lateral margin of the bone defects under MXene films at high magnification. Blue arrows mark the MXene films. Scale bars: 200 μ m.

Abbreviation: NB, new bone.

obvious inflammatory and toxic side effects, indicating their safety and high biocompatibility in vivo. A rat calvarial defect model reveals that MXene films promote early osteogenesis, mineralization and bone regeneration. Collectively, these findings provide evidence that $\text{Ti}_3\text{C}_2\text{T}_x$ MXene is highly biocompatible in vitro and in vivo with sufficient osteoinductivity as an emerging 2D material for bone tissue engineering and GBR therapy.

Acknowledgment

This study was supported by The National Key Research and Development Program of China (2016YFA0201703/2016YFA0201700).

Disclosure

The authors report no conflicts of interest in this work.

References

- Hämmerle CH, Karring T. Guided bone regeneration at oral implant sites. *Periodontol 2000*. 1998;17(1):151–175. doi:10.1111/j.1600-0757.1998.tb00132.x
- Retzepi M, Donos N. Guided bone regeneration: biological principle and therapeutic applications. *Clin Oral Implants Res*. 2010;21(6):567–576. doi:10.1111/j.1600-0501.2010.01922.x
- Elgali I, Omar O, Dahlin C, Thomsen P. Guided bone regeneration: materials and biological mechanisms revisited. *Eur J Oral Sci*. 2017;125(5):315–337. doi:10.1111/eos.12364
- Yang F, Both SK, Yang X, Walboomers XF, Jansen JA. Development of an electrospun nano-apatite/PCL composite membrane for GTR/GBR application. *Acta Biomater*. 2009;5(9):3295–3304. doi:10.1016/j.actbio.2009.05.023
- Bottino MC, Thomas V, Schmidt G, et al. Recent advances in the development of GTR/GBR membranes for periodontal regeneration—a materials perspective. *Dent Mater*. 2012;28(7):703–721. doi:10.1016/j.dental.2012.04.022
- Stevens MM. Biomaterials for bone tissue engineering. *Mater Today*. 2008;11(5):18–25. doi:10.1016/S1369-7021(08)70086-5
- Pinheiro ALB, Gerbi MEM, de Assis Limeira F, et al. Bone repair following bone grafting hydroxyapatite guided bone regeneration and infra-red laser photobiomodulation: a histological study in a rodent model. *Lasers Med Sci*. 2009;24(2):234–240. doi:10.1007/s10103-008-0556-0
- Kim K-H, Jeong L, Park H-N, et al. Biological efficacy of silk fibroin nanofiber membranes for guided bone regeneration. *J Biotechnol*. 2005;120(3):327–339. doi:10.1016/j.jbiotec.2005.06.033
- Ming G, Yunsong L, Tong C, et al. Is graphene a promising nano-material for promoting surface modification of implants or scaffold materials in bone tissue engineering? *Tissue Eng Part B Rev*. 2014;20(5):477–491. doi:10.1089/ten.teb.2013.0638

10. Goenka S, Sant V, Sant S. Graphene-based nanomaterials for drug delivery and tissue engineering. *J Control Release*. 2014;173:75–88. doi:10.1016/j.jconrel.2013.10.017
11. Nayak TR, Andersen H, Makam VS, et al. Graphene for controlled and accelerated osteogenic differentiation of human mesenchymal stem cells. *ACS Nano*. 2011;5(6):4670–4678. doi:10.1021/nn200500h
12. Lu J, He YS, Cheng C, et al. Self-supporting graphene hydrogel film as an experimental platform to evaluate the potential of graphene for bone regeneration. *Adv Funct Mater*. 2013;23(28):3494–3502. doi:10.1002/adfm.201203637
13. Lu J, Cheng C, He YS, et al. Multilayered graphene hydrogel membranes for guided bone regeneration. *Adv Mater*. 2016;28(21):4025–4031. doi:10.1002/adma.201505375
14. Naguib M, Kurtoglu M, Presser V, et al. Two-dimensional nanocrystals produced by exfoliation of Ti₃AlC₂. *Adv Mater*. 2011;23(37):4248–4253. doi:10.1002/adma.201102306
15. Naguib M, Mashtalir O, Carle J, et al. Two-dimensional transition metal carbides. *ACS Nano*. 2012;6(2):1322–1331. doi:10.1021/nn204153h
16. Naguib M, Mochalin VN, Barsoum MW, Gogotsi Y. 25th anniversary article: mXenes: a new family of two-dimensional materials. *Adv Mater*. 2014;26(7):992–1005. doi:10.1002/adma.201304138
17. Peng Q, Guo J, Zhang Q, et al. Unique lead adsorption behavior of activated hydroxyl group in two-dimensional titanium carbide. *J Am Chem Soc*. 2014;136(11):4113–4116. doi:10.1021/ja500506k
18. Anasori B, Lukatskaya MR, Gogotsi Y. 2D metal carbides and nitrides (MXenes) for energy storage. *Nat Rev Mater*. 2017;2(2). doi:10.1038/natrevmats.2016.98
19. Ling Z, Ren CE, Zhao M-Q, et al. Flexible and conductive MXene films and nanocomposites with high capacitance. *Proc Natl Acad Sci*. 2014;111(47):16676–16681. doi:10.1073/pnas.1414215111
20. Ghidui M, Lukatskaya MR, Zhao M-Q, Gogotsi Y, Barsoum MW. Conductive two-dimensional titanium carbide ‘clay’ with high volumetric capacitance. *Nature*. 2014;516(7529):78. doi:10.1038/nature13970
21. Nasrallah GK, Al-Asmakh M, Rasool K, Mahmoud KA. Ecotoxicological assessment of Ti₃C₂Tx (MXene) using a zebrafish embryo model. *Environ Sci Nano*. 2018;5(4):1002–1011. doi:10.1039/C7EN01239J
22. Jastrzębska A, Szuplewska A, Wojciechowski T, et al. In vitro studies on cytotoxicity of delaminated Ti₃C₂ MXene. *J Hazard Mater*. 2017;339:1–8. doi:10.1016/j.jhazmat.2017.06.004
23. Lin H, Gao S, Dai C, Chen Y, Shi J. A two-dimensional biodegradable niobium carbide (MXene) for photothermal tumor eradication in NIR-I and NIR-II biowindows. *J Am Chem Soc*. 2017;139(45):16235–16247. doi:10.1021/jacs.7b07818
24. Rasool K, Helal M, Ali A, Ren CE, Gogotsi Y, Mahmoud KA. Antibacterial Activity of Ti₃C₂Tx MXene. *ACS Nano*. 2016;10(3):3674–3684. doi:10.1021/acsnano.6b00181
25. Huang K, Li Z, Lin J, Han G, Huang P. Two-dimensional transition metal carbides and nitrides (MXenes) for biomedical applications. *Chem Soc Rev*. 2018;47(14):5109–5124. doi:10.1039/C7CS00838D
26. Wang F, Yang C, Duan M, Tang Y, Zhu J. TiO₂ nanoparticle modified organ-like Ti₃C₂ MXene nanocomposite encapsulating hemoglobin for a mediator-free biosensor with excellent performances. *Biosens Bioelectron*. 2015;74:1022–1028. doi:10.1016/j.bios.2015.08.004
27. Chen X, Sun X, Xu W, et al. Ratiometric photoluminescence sensing based on Ti₃C₂ MXene quantum dots as an intracellular pH sensor. *Nanoscale*. 2018;10(3):1111–1118. doi:10.1039/C7NR06958H
28. Rasool K, Mahmoud KA, Johnson DJ, Helal M, Berdiyev GR, Gogotsi Y. Efficient antibacterial membrane based on two-dimensional Ti₃C₂Tx (MXene) nanosheets. *Sci Rep*. 2017;7(1):1598. doi:10.1038/s41598-017-01714-3
29. Yu X, Cai X, Cui H, Lee S-W, Yu X-F, Liu B. Fluorine-free preparation of titanium carbide MXene quantum dots with high near-infrared photothermal performances for cancer therapy. *Nanoscale*. 2017;9(45):17859–17864. doi:10.1039/C7NR05997C
30. Xu B, Zhu M, Zhang W, et al. Ultrathin MXene-micropattern-based field-effect transistor for probing neural activity. *Adv Mater*. 2016;28(17):3333–3339. doi:10.1002/adma.201504657
31. Dai C, Lin H, Xu G, Liu Z, Wu R, Chen Y. Biocompatible 2D titanium carbide (MXenes) composite nanosheets for pH-responsive MRI-guided tumor hyperthermia. *Chem Mater*. 2017;29(20):8637–8652. doi:10.1021/acs.chemmater.7b02441
32. Chen K, Chen Y, Deng Q, et al. Strong and biocompatible poly (lactic acid) membrane enhanced by Ti₃C₂Tz (MXene) nanosheets for Guided bone regeneration. *Mater Lett*. 2018;229:114–117. doi:10.1016/j.matlet.2018.06.063
33. Alhabeab M, Maleski K, Anasori B, et al. Guidelines for synthesis and processing of two-dimensional titanium carbide (Ti₃C₂Tx MXene). *Chem Mater*. 2017;29(18):7633–7644. doi:10.1021/acs.chemmater.7b02847
34. Anderson SB, Lin CC, Kuntzler DV, Anseth KS. The performance of human mesenchymal stem cells encapsulated in cell-degradable polymer-peptide hydrogels. *Biomaterials*. 2011;32(14):3564–3574. doi:10.1016/j.biomaterials.2011.01.064
35. Schmitz JP, Hollinger JO. The critical size defect as an experimental model for craniomandibulofacial nonunions. *Clin Orthop Relat Res*. 1986;(205):299–308. doi:10.1097/00003086-198604000-00036
36. Doube M, Klosowski MM, Arganda-Carreras I, et al. BoneJ: free and extensible bone image analysis in ImageJ. *Bone*. 2010;47(6):1076–1079. doi:10.1016/j.bone.2010.08.023
37. Zhang W, Feng C, Yang G, et al. 3D-printed scaffolds with synergistic effect of hollow-pipe structure and bioactive ions for vascularized bone regeneration. *Biomaterials*. 2017;135:85–95. doi:10.1016/j.biomaterials.2017.05.005
38. Dalby MJ, Gadegaard N, Tare R, et al. The control of human mesenchymal cell differentiation using nanoscale symmetry and disorder. *Nat Mater*. 2007;6(12):997. doi:10.1038/nmat2013
39. Ponsionnet L, Reybier K, Jaffrezic N, et al. Relationship between surface properties (roughness, wettability) of titanium and titanium alloys and cell behaviour. *Mater Sci Eng C*. 2003;23(4):551–560. doi:10.1016/S0928-4931(03)00033-X
40. Peng R, Yao X, Cao B, Tang J, Ding J. The effect of culture conditions on the adipogenic and osteogenic inductions of mesenchymal stem cells on micropatterned surfaces. *Biomaterials*. 2012;33(26):6008–6019. doi:10.1016/j.biomaterials.2012.05.010
41. Wang D, Christensen K, Chawla K, Xiao G, Krebsbach PH, Franceschi RT. Isolation and characterization of MC3T3-E1 preosteoblast subclones with distinct in vitro and in vivo differentiation/mineralization potential. *J Bone Miner Res*. 1999;14(6):893–903. doi:10.1359/jbmr.1999.14.6.893
42. Quarles LD, Yohay DA, Lever LW, Caton R, Wenstrup RJ. Distinct proliferative and differentiated stages of murine MC3T3-E1 cells in culture: an in vitro model of osteoblast development. *J Bone Miner Res*. 1992;7(6):683–692. doi:10.1002/jbmr.5650070613
43. Ren CE, Hatzell KB, Alhabeab M, Ling Z, Mahmoud KA, Gogotsi Y. Charge- and size-selective ion sieving through Ti₃C₂Tx MXene membranes. *J Phys Chem Lett*. 2015;6(20):4026–4031. doi:10.1021/acs.jpcclett.5b01895
44. Zhang X, Zhang C, Lin Y, et al. Nanocomposite membranes enhance bone regeneration through restoring physiological electric microenvironment. *ACS Nano*. 2016;10(8):7279–7286. doi:10.1021/acsnano.6b02247
45. Zhang CJ, Pinilla S, McEvoy N, et al. Oxidation stability of colloidal two-dimensional titanium carbides (MXenes). *Chem Mater*. 2017;29(11):4848–4856. doi:10.1021/acs.chemmater.7b00745
46. Ding M, Hvid I. Quantification of age-related changes in the structure model type and trabecular thickness of human tibial cancellous bone. *Bone*. 2000;26(3):291–295. doi:10.1016/S8756-3282(99)00281-1

International Journal of Nanomedicine

Dovepress

Publish your work in this journal

The International Journal of Nanomedicine is an international, peer-reviewed journal focusing on the application of nanotechnology in diagnostics, therapeutics, and drug delivery systems throughout the biomedical field. This journal is indexed on PubMed Central, MedLine, CAS, SciSearch[®], Current Contents[®]/Clinical Medicine,

Journal Citation Reports/Science Edition, EMBase, Scopus and the Elsevier Bibliographic databases. The manuscript management system is completely online and includes a very quick and fair peer-review system, which is all easy to use. Visit <http://www.dovepress.com/testimonials.php> to read real quotes from published authors.

Submit your manuscript here: <https://www.dovepress.com/international-journal-of-nanomedicine-journal>